Lab Report

# Engineering *Escherichia coli* to produce *Tenebrio molitor* and *Lolium perenne* antifreeze proteins as a road salt alternative\*

Arsh Goyal, Nicole Pae, James Vacca, and Lingzhen Wang - Western Reserve Academy, Hudson, OH

Reviewed on 3 May 2025; Accepted on 9 June 2025; Published on 27 October 2025

Annual U.S. vehicle crashes on snowy and icy roads result in more than 1,300 deaths and 116,800 injuries. However, using chemical road salt to prevent accidents has negative consequences, including corrosion and nearby water contamination. Our more eco-friendly design utilizes naturally occurring antifreeze proteins (AFPs) to prevent ice formation on road surfaces. The aim of this project was to construct two plasmids, one expressing an AFP from Lolium perenne (perennial ryegrass) and one from Tenebrio molitor (mealworm). Both genes are controlled by inducible promoters in the Escherichia coli chassis. Proteins were extracted from the transformed E. coli using cell lysis, centrifugation, and solubilization to release the inclusion bodies containing the proteins. AFPs were then purified through affinity chromatography to ensure high purity for functionality and stability tests. In preliminary transformations, robust colony growth was observed for the T. molitor AFP construct, whereas no colonies formed for the L. perenne construct, indicating differential cloning or selection efficiency that guided our next optimization steps. The application of these AFPs offers a sustainable and eco-friendly alternative to traditional road salt, mitigating environmental damage while preventing risks of icy roads.

Keywords: Antifreeze proteins, sustainability, Escherichia coli











inter roads create serious hazards for drivers around the world. In the U.S. alone, icy and snowy conditions contribute to over 1,300 deaths and more than 116,800 injuries from vehicle crashes each year (American Highway Users Alliance, 2018). To make roads safer during the colder months, the U.S. spreads between 15 and 32 million tons of road salt annually (Carry Institute of Ecosystem Studies, n.d.). This salt, mainly sodium chloride, works by lowering water's freezing point, helping ice melt even when it's below freezing. Despite its effectiveness, road salt comes with major downsides. It can contaminate water supplies, disrupt ecosystems, and corrode vehicles and infrastructure (Pieper et al., 2018). Because of these issues, researchers and transportation departments have been exploring safer and more sustainable alternatives.

Management of Icy Roads

<sup>\*</sup> The authors were mentored by Rebecca Meyer from Massachusetts Institute of Technology and Beth Pethel from Western Reserve Academy. Please direct correspondence to: pethelb@wra.net. This is an Open Access article, which was copyrighted by the authors and published by BioTreks in 2025. It is distributed under the terms of the Creative Commons Attribution License, which permits non-commercial re-use, distribution, and reproduction in any medium, provided the original work is properly cited.

The management of icy roads is conducted through two distinct but complementary processes: anti-icing and de-icing. Anti-icing is a proactive approach where a liquid solution is applied to the pavement before snowfall occurs. Although effective under moderate snowfall conditions, anti-icing treatments are vulnerable to heavy precipitation and rapid temperature changes. High levels of snowfall can dilute or wash away the anti-icing products, rendering them less effective (Federal Highway Administration [FHWA]. 1996). effectiveness Additionally. anti-icing diminishes when temperatures drop below the eutectic point of the chemical solution being used. In such cases, de-icing becomes necessary. De-icing is a reactive process applied after snow or ice has bonded to the pavement. It involves the use of chemical

restoring road safety in more severe winter conditions.

#### Environmental concerns

While effective, anti-icing and de-icing chemicals such as magnesium chloride and sodium chloride pose several environmental and structural risks, as explained in Figure 1. For example, liquid magnesium chloride is ineffective below -15°C due to its limited capacity to lower the freezing point sufficiently. Moreover, when precipitation persists, road friction decreases drastically, increasing accident risks despite anti-icing measures (Mainroad, n.d.). Liquid brine—a 23% salt, 77% water solution—is more affordable and works in temperatures as low as -29°C, but corrodes infrastructure and pollutes ecosystems ((Lilek, 2017; Mainroad,

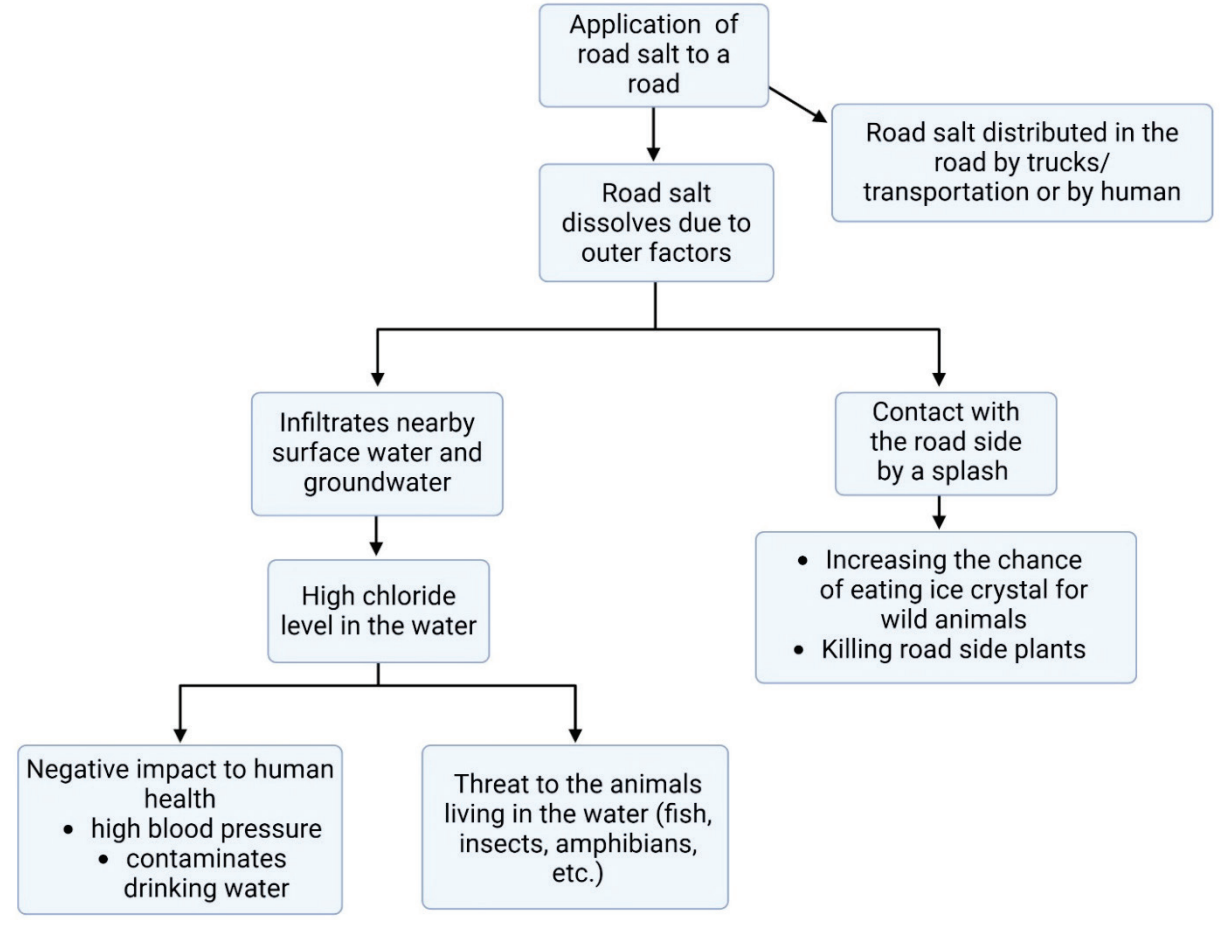


Figure 1. Environmental and human impacts of road salt application. (Guidelines for the selection of snow and ice control materials to mitigate environmental impacts, 2007). Created with Biorender.com.

agents or mechanical methods to break the ice-pavement bond, allowing for removal and

n.d.). Sodium chloride harms freshwater species at just 100 mg/L and accumulates

over time, degrading water quality (Corsi, De Cicco, Lutz, & Hirsch, 2015).

#### Cost

The most common product used in the deicing step is road salt. Studies show the importance of de-icers in improving road surface conditions. In 2013, a mere 10% improvement in surface friction could lead to a 20% reduction in crashes (American Highway Users Alliance, 2018). Road salt is the most affordable and efficient de-icer to vehicle safety during ensure American roads and highways use road salt, which has been proven to reduce collisions by up to 88% and injuries by 85%; on fourlane roads, this estimate is raised to 93% (American Highway Users Alliance, 2018). The economic impact of road closures due to inclement weather, including costs associated with snow plowing and removal, can range from \$300 to \$700 million. In this context, applying road salt represents a relatively modest investment. The cost of salt application pays for itself within the first four hours, as road users receive direct benefits of \$6.50 for every \$1.00 spent (American Highway Users Alliance, 2018). As of today, road salt remains the most cost-effective option for ensuring road safety, but improvements are still needed.

#### Our solution

Considering the environmental concerns, health risks, and high costs associated with these de-icing products, an environmentally friendly and cost-effective alternative is needed in the long run. This project aims to find a cleaner alternative to chemical road salt by using antifreeze proteins (AFPs). The potential benefits are preventing corrosion caused by road salt and improving road longevity with a bioengineered *E. coli* strain that combines AFPs from multiple species.

Tenebrio molitor, a strain of yellow mealworm beetle, generates two thermal hysteresis proteins (THPs), Cys-rich and Thrrich (Graham et al., 2000). Thermal hysteresis refers to the phenomenon where the freezing point of a substance is lowered without interfering with its melting temperature. THPs are types of AFPs that

lower the freezing point of the hemolymph of T. molitor, enabling its survival in subzero temperatures. Organisms, including insects, fish, and plants, can synthesize THPs when they live in environments where the temperature is consistently below 0°C (32°F). Previous research on THPs involved the isolation of one functional THP, xvlomannan, from the freeze-tolerant beetle Upis ceramides through an ice affinity protocol (Walters et al., 2009), which marks the first instance of an antifreeze substance isolated from a freeze-tolerant animal. This groundbreaking finding paves the way for our design as we explore the real-world application of freeze tolerance—the ability of organisms to survive in conditions where their body fluids freeze —in the context of mass protein production for environmental

Lolium perenne produces an AFP (LpAFP) of approximately 118 amino acids featuring semi-conserved repeats folding into a β-roll structure that enables it to bind ice and inhibit ice crystal growth (Kuiper et al., 2001). Homologous domains have been identified in other Pooideae grasses such as wheat and barley, but LpAFP is uniquely abundant in perennial ryegrass Expressed Sequence Tag (EST) and Bacterial Artificial Chromosome (BAC) libraries, where some variants have demonstrated measurable iceactivity when heterologously expressed (Middleton et al., 2009). In plants, LpAFP has been stably integrated and transcribed in transgenic tomato lines (Balamurugan et al., 2018). Additionally, bacterial expression systems have yielded functional LpAFP that can be purified (Pudney et al., 2003). These studies highlight the practicality of expressing LpAFP genes in heterologous species.

AFPs prevent ice formation by attaching to the ice surface, hindering water molecules from attaching to ice-binding sites, which are specific places on the ice nucleus. Ice crystals typically grow in a symmetrical and uniform manner as water molecules continue to freeze. However, as detailed in Figure 2, the interference of binding AFPs alters this process by inducing the formation of a convex interface on the side facing the surrounding liquid (Hakim et al., 2013). This AFP-induced convexity changes the normal

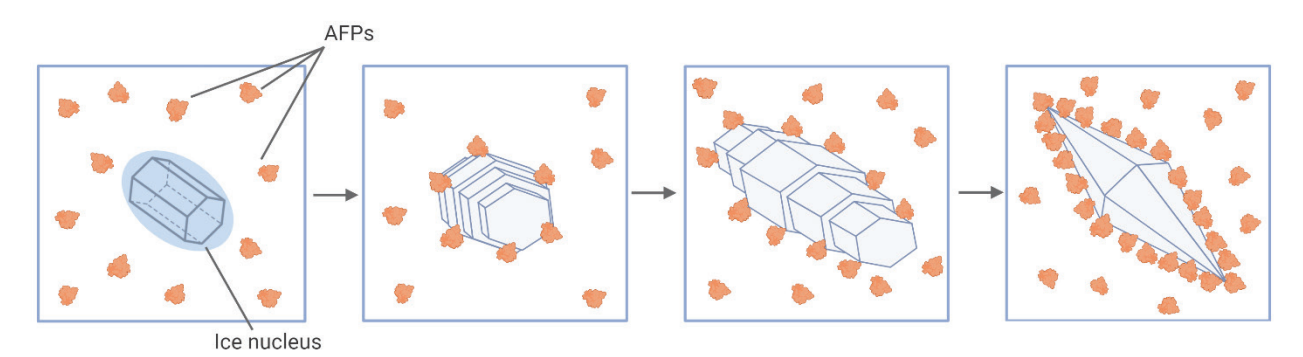


Figure 2. Mechanism of AFPs interfering with ice formation (Kondo, H., 2012). Created using BioRender.com.

growth morphology of the ice crystal. According to the Gibbs-Thomson-Herring effect, those convex surfaces are thermodynamically less stable and unfavorable for further ice extension, as depicted in Figure 3 (Gharib et al., 2022).

The structural types of AFP determine ability to bind to crystallographic ice planes. This binding occurs through a region, known as the icebinding site (IBS), on the AFP. The IBS is believed to organize water molecules adjacent to AFP into a conformation that mimics the lattice arrangement found in ice molecular structure, but without inducing actual ice formation (Kondo, 2012). By prearranging these water molecules into an icelike pattern, AFPs effectively prepare their binding interface to complement a specific ice plane (Eskandari et al., 2020). The IBS then aligns with a corresponding plane on the

ice surface upon encountering an ice crystal. The molecular complementarity between the water molecule arrangement at the IBS and the atomic structure of the targeted ice plane facilitates this attachment. Different AFPs exhibit different binding preferences depending on their structures. For instance, Type 1 AFPs from the winter flounder preferentially bind to the pyramidal and secondary prism planes of ice, whereas hyperactive AFPs from the Antarctic bacterium Flavobacterium frigoris PS1 target the basal plane of ice crystals (Kim et al., 2017). These matchings replace water binding that causes further ice crystal growth at the site and enables the AFP to selectively adhere to ice planes (Eskandari et al., 2020).

Thus, harnessing the precise ice-plane specificity of AFPs offers a promising, biodegradable strategy for ice-prevention. Conventional de-icing agents pose

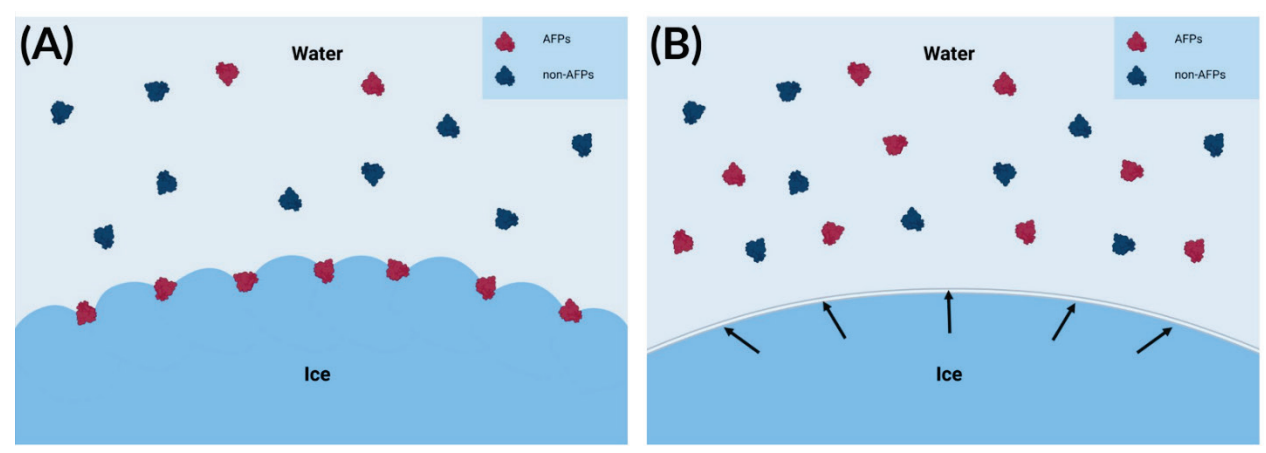


Figure 3. Gibbs-Thomson-Herring effect and the mechanism of AFPs.(A) AFPs bind to the advancing ice front, while non-AFPs remain unbound. AFP binding increases the curvature of the ice surface, thereby inhibiting further ice growth (Kuiper et al., 2015). (B) A mixture of AFPs and non-AFPs near the ice front (Kuiper et al., 2015). Created using BioRender.com.

environmental impacts, potential health hazards, and substantial economic costs, making the need to develop a more sustainable and cost-effective alternative pressing. By engineering an *E. coli* strain DH5-α to produce AFPs derived from two specific sources, *T. molitor* and *L. perenne*, this project aims to utilize biodegradable AFPs to replace chemical road salts.

We envision our product to be applied as a product with the mixture of two purified *T. moliter* AFP and LP-AFP blend into an aqueous spray containing buffering agents, a food-grade surfactant to promote even spreading, and a stabilizer to preserve protein activity during storage and freezing. This reversible protein coating on pavement surfaces will bind nascent ice nuclei and prevent adherence without corroding underlying concrete or metal infrastructure.

Although AFP production is more expensive on a per-kilogram basis than bulk road salt, several factors could make our protein-based spray more cost-effective over its lifetime. With industrial fermentation of recombinant E. coli in optimized bioreactors using inexpensive carbon sources (e.g., glycerol or corn steep liquor), downstream costs for purified AFP can fall to the low tens of dollars per kilogram and continue to decline with process improvements and economies of scale (Puetz & Wurm, 2019). In addition, AFPs act at micromolar concentrations, so a single kilogram of protein can treat thousands of square meters of pavement versus one to two tons of salt per kilometer of road. By reducing corrosion and infrastructure repair costs, this bio-spray can generate net savings even at moderate protein production costs.

# **Materials and methods**

In this study, we engineered E. coli DH5- $\alpha$  to express two AFPs by cloning synthesized gene inserts into arabinose- and tetracycline-induced plasmid backbones, followed by transformation and antibiotic-selective cultivation. Recombinant strains were then grown in defined media. All materials used in this study were sourced from established commercial suppliers. All bacterial cultures were grown in Luria-Bertani (LB) medium

with the appropriate antibiotics, and the transformation plates were incubated overnight at 37°C.

#### LB preparation (LB Fischer)

LB broth and Luria Agar (LA) were prepared using LB and LA powders (Fisher Scientific). To prepare LB broth, 2.5 g of LB powder was mixed with 100 mL of room-temperature deionized water. The mixture was stirred thoroughly until the powder was completely dissolved. Once fully dissolved, the LB medium was sterilized by autoclaving at 121°C under 15 psi of pressure for 15 minutes.

For the preparation of LA, 3.5 grams of LA powder was added to 100 mL of room-temperature deionized water. The solution was brought to a boil while being continuously stirred to ensure that the components dissolved completely. Once fully dissolved, the LA medium was sterilized by autoclaving at 121°C under 15 psi of pressure for 15 minutes.

# Stock solution preparation (Chloramphenicol and Kanamycin)

Antibiotic stock solutions were prepared using chloramphenicol and kanamycin powders (GoldBio) and then filtered through 0.2 µm syringe filters (Fisher Scientific).

#### Chloramphenicol (GoldBio)

To prepare the chloramphenicol stock solution, 250 milligrams of chloramphenicol powder were dissolved in 10 milliliters of 70% ethanol. The solution was mixed thoroughly with a vortex until it was fully dissolved. The resulting solution was then passed through a 0.2  $\mu$ m syringe filter to remove any contaminants. This filtered stock solution was added to the media at a final working concentration of 50  $\mu$ g/mL.

## Kanamycin (GoldBio)

For the kanamycin stock, 5 milligrams of kanamycin was dissolved in 10 milliliters of distilled water. The solution was vortexed to ensure complete dissolution. As with the

chloramphenicol solution, it was then filtered through a 0.2  $\mu m$  syringe filter to remove contaminants. The stock was used in media at a final concentration of 50  $\mu g/mL$ .

Bacterial culture growth & plasmid extractions

The two plasmid vectors, pUS212 (Addgene) and pBAD18-Kan (ATCC), with selectable markers chloramphenical and kanamycin, respectively, were grown in LB medium containing antibiotics.

A single colony of DH5- $\alpha$  containing each desired plasmid was picked from a freshly streaked plate and inoculated in LB medium containing the appropriate selectable marker antibiotic. The bacterial cells were harvested by centrifugation at 8000 rpm in a microcentrifuge for three minutes at room temperature.

Miniprep procedures (QIAprep Spin Miniprep Kit High-Yield)

Bacterial DNA was extracted using the QIAprep Spin Miniprep Kit High-Yield (Qiagen). according to manufacturer's recommendations. Briefly, pelleted bacterial cells were resuspended in a 250 µL buffer P1 and transferred to a microcentrifuge tube. RNase A was added to Buffer P1 for a final concentration of 100 µg/mL. To initiate lysis, 250 µL of buffer P2 was mixed thoroughly and allowed to react for three minutes. Subsequently, 350 µL of buffer N3 was added to the pelleted bacterial cells and mixed immediately. After centrifuging for 10 minutes, 800 µL of supernatant was applied to the Qiagen 2.0 spin column, which was fixed on a 1.5 mL microcentrifuge tube, and then the tube was centrifuged for 30 seconds. Flow-through was discarded. The spin column was washed with 500 µL Buffer PB and centrifuged for 30 seconds; the flowthrough was discarded. The spin column was then washed with 750 µL Buffer PE and centrifuged for thirty seconds; the flow-through was discarded. The spin column was centrifuged for one minute to remove the residual wash buffer. The spin column was then placed in a clean 1.5 mL microcentrifuge tube. 60 µL of Buffer EB was added to the

center of the spin column. It was left to stand for one minute, then centrifuged for one minute. All centrifugation was carried out at 13,000 rpm.

Verify the plasmid DNA existence and the optical density

To measure the DNA concentrations of minipreps using drop optical density (OD), each of the DNA samples was placed directly on the measurement pedestal of a BlueRay 1000 EzDrop Micro-Volume spectrophotometer. The device measures absorbance at 260 nm, the wavelength at which nucleic acids absorb UV light. After blanking the instrument with the appropriate buffer, the DNA sample was loaded, and the resulting absorbance value was used to calculate concentration based on the Beer-Lambert law. The purity of the sample was also assessed using the A260/A280 ratio.

#### Insert-DNA design and synthesis

The insert sequences were retrieved from GenBank, while the plasmid backbone sequences were obtained from Addgene. Insert gene sequences, THP YL-1 genes from *T. moliter* and the LpAFP IRI3 protein gene, were synthesized by Twist Bioscience and cloned using restriction enzymes (NheI, SalI, SpeI, and PstI).

After importing the plasmid sequences into Benchling, two unique, non-repetitive restriction enzymes—each present only within the multiple cloning site—were selected for each construct. For pBAD18-Kan, NheI was chosen for the 5' end and SalI for the 3' end. For pUS212, SpeI and PstI were selected for the 5' and 3' ends, respectively. To facilitate cloning, the LP-AFP gene insert was flanked with NheI and SalI restriction sites, while the *T. molitor* gene insert was flanked with SpeI and PstI sites. Ribosome binding sites (RBS) were incorporated upstream of each gene insert to ensure optimal expression. Spacer sequences were added between the restriction sites and coding regions to prevent interference with essential genetic elements and to improve restriction enzyme accessibility. finalized insert sequences were synthesized

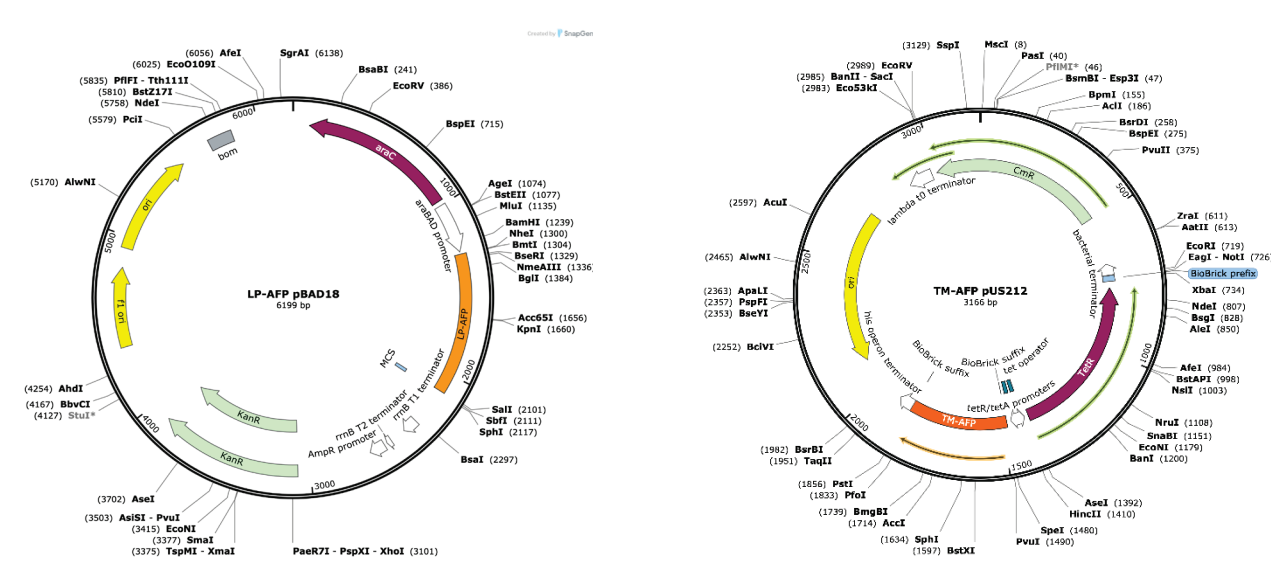


Figure 4. Maps of the two synthesized plasmid constructs used for AFP expression. (Left) LP-AFP pBAD18-Kan: This 6199 bp plasmid carries the L. perenne AFP (LP-AFP) gene under control of the arabinose-inducible araBAD promoter, with a kanamycin resistance gene (KanR) for selection. The LP-AFP insert is flanked by Nhel and Sall restriction sites and includes a ribosome RBS upstream of the coding sequence. (Right) TM-AFP pUS212: This 3166 bp plasmid contains the T. molitor AFP (TM-AFP) gene driven by the tetracycline-inducible tet/tetR promoter. The insert is flanked by Spel and Pstl restriction sites and also includes an RBS for translation initiation. Chloramphenicol resistance (CmR) serves as the selection marker. Both constructs were designed using SnapGene and are ready for downstream transformation and expression optimization in E. coli.

and purchased from Twist Bioscience; specific genetic components are shown in Figure 4.

# Double digestion - stock & experimental molarity and quantity calculation

In order to create complementary, nonidentical ends that force the insert into the plasmid in the correct orientation, double digestion steps were used to cut both the vectors and the inserts. Double digestions were performed following the NEB Cloner Double Digest Protocol, version 1.14.2. According to the protocol, 1 µg of DNA is required for each restriction digest. Based on Drop OD measurements, the concentrations were  $12.33 \text{ ng/}\mu\text{L}$ pUS212 for 28.19 ng/µL for pBAD18-Kan. To obtain 1 μg of DNA, 81.1 μL of pUS212 and 35.47 µL of pBAD18-Kan were required. However, due to the 50 µL volume limit of the restriction digest protocol, 43 µL of pUS212 and 35.5 µL of pBAD18-Kan were used in the final reaction setup. Using roughly half of the intended DNA

proportionally reduced the amount of cut vector for ligation.

The synthesized insert DNAs from Twist Bioscience were supplied at a concentration of 25 ng/ $\mu$ L, requiring 40  $\mu$ L of each insert per digestion. Given the limited volume available, each insert was resuspended in 10  $\mu$ L of nuclease-free water, and 5  $\mu$ L was used for digestion.

After gently pipetting and mixing the reagents listed in Table 1, the digests were incubated at 37°C for 10 minutes. For the

Table 1. The reaction components of restriction digest for pBAD18-Kan, L. perenne insert, pUS212, and T. molitor insert.

mocrt.				
	pBAD18- Kan	L. perenne insert	pUS212	T. molitor insert
DNA (µL)	35.5	5	43	5
R Cutsmart Buffer (µL)	5	5	5	5
Enzyme 1 (µL)	1 µL Nhel	1 µL Nhel	1 µL Spel	1 µL Spel
Enzyme 2 (µL)	1 μL Sall	1 μL Sall	1 μL Pstl	1 µL PstI
Nuclease- free water (µL)	7.5	38	0	38

pBAD18-Kan plasmid and *L. perenne* AFP insert, restriction enzymes were subsequently heat-inactivated at 80°C for 20 minutes. In the case of pUS212 and the *T. molitor* AFP insert, the reaction mixtures proceeded directly to Monarch DNA Cleanup after incubation.

T. molitor / pUS212 cleanup – NEB Monarch Spin PCR & DNA Cleanup Kit (5 μg)

Since PstI-HF could not be inactivated by heat, we decided to use the Monarch Spin PCR & DNA Cleanup Kit (5 µg) for the digested T. molitor sample and the pUS212 sample, which contains PstI-HF. 250 µL of Monarch Buffer BZ was added to 50 µL of the digested T. molitor sample from the previous step. The mixture was then mixed by pipetting up and down or flicking the tube. After the Monarch Spin Column S1A was inserted into the Monarch Spin Collection Tube, the sample was loaded onto the column. After centrifuging for 1 minute, the flow-through was discarded. Then, the column was re-inserted into a new collection tube. It was washed by adding 200 µL of Monarch Buffer WZ and centrifuging for 1 minute. The wash was repeated one more time. Then, the column was transferred to a sterile 1.5 mL microfuge tube. 15 µL of Monarch Buffer EY was added to the center of the Matrix to elute DNA. After letting it sit for 1 minute, the tube was centrifuged for 1 minute.

The whole process was repeated for the pUS212 sample.

#### Plasmid ligation

The NEB Quick Ligation Kit was used for both plasmid constructs. To calculate the required vector volumes and insert DNA, we utilized the NEBio Ligation Calculator. For 50 ng of the pBAD18-Kan vector, 22.26 ng of *L. perenne* AFP insert DNA was needed to achieve a 1:3 vector-to-insert molar ratio. Given that the concentrations of pBAD18-Kan and *L. perenne* AFP insert were 20 ng/µL and 2.5 ng/µL, respectively, we used 2.5 µL of vector and 9 µL of insert. Since the original protocol required that the combined

volume of vector and insert DNA be less than 9  $\mu$ L, we doubled the total reaction volume. The final components of the ligation reaction for pBAD18-Kan and *L. perenne* AFP insert are shown in Table 2.

Similarly, we calculated the required volumes for the pUS212 vector and T. molitor AFP insert using the NEBio Ligation Calculator. For 50 ng of pUS212, 20.19 ng of insert DNA was needed. Given the post-cleanup concentrations of 35.3 ng/ $\mu$ L for the pUS212 vector and 8.33 ng/ $\mu$ L for the T. molitor AFP insert, the volumes used were 1.5  $\mu$ L and 2.5  $\mu$ L, respectively. The final components of this ligation reaction are also detailed in Table 2.

After preparing the ligation reactions in two microcentrifuge tubes, we gently mixed the contents and incubated them at room temperature for 5 minutes, followed by storage at  $-20^{\circ}$ C.

Table 2. The reaction components for pBAD18-Kan and L. perenne insert ligation and pUS212 and T. molitor insert ligation.

	pBAD18-Kan and L. perenne insert	pUS212 and <i>T. molitor</i> insert
Total reaction volume (μL)	40	20
Quick Ligase Reaction Buffer 2X (μL)	20	20
Vector DNA (µL)	2.5	1.5
Insert DNA (µL)	9	2.5
Nuclease-free water (µL)	6.5	5
Quick ligase (µL)	2	1

#### DH5-α transformation

Transformation recovery was carried out using Super Optimal broth with Catabolite repression (SOC) medium (Thermo Fisher). The competent DH5- $\alpha$  cells from Thermo Fisher (Catalog number EC0112) were thawed on wet ice. Four 1.5 mL polypropylene microcentrifuge tubes were also placed on wet ice. After gently mixing the cells, 50  $\mu$ L aliquots were dispensed into each chilled tube. Into two of the tubes, 5  $\mu$ L of ligated pUS212 with the *T. molitor* insert was added. Into the other two tubes, 5  $\mu$ L of ligated pBAD18-Kan with the *L. perenne* insert was added.

After adding the ligated DNA samples to the competent DH5- $\alpha$  cells, the tubes were gently mixed and incubated on ice for 30 minutes. Then, they were heat-shocked for 30 seconds in a 42°C water bath. The tubes were

not mixed or shaken. The cells were then incubated on ice for 2 minutes. A room-temperature SOC medium was then added, and the tubes were placed horizontally in a shaking incubator at 225 rpm for 1 hour at 37°C.

Following incubation, three plates containing  $E.\ coli$  transformed with pUS212 and the  $T.\ molitor$  insert were plated on LA containing chloramphenical at volumes of 20  $\mu$ L, 100  $\mu$ L, and 200  $\mu$ L, respectively. Four plates containing  $E.\ coli$  transformed with pBAD18-Kan and the  $L.\ perenne$  insert were plated on LA containing kanamycin at two volumes: 20  $\mu$ L and 200  $\mu$ L (two plates per concentration). The plates were incubated overnight at 37°C.

#### Laboratory and environmental safety

All experimental work was conducted under Biosafety Level (BSL-1) guidelines with the use of personal protective equipment (lab coats, nitrile gloves, and safety goggles). All waste materials and consumables were decontaminated and autoclaved before disposal. Liquid waste streams containing antibiotics or IPTG were collected separately and treated with bleach to inactivate residual antibiotics before release. To minimize release of environmental genetically modified organisms, all transformations and plate incubations were performed inside a dedicated containment area, and no live cultures were drained.

#### Gel electrophoresis

Agarose gels (2% w/v) were prepared using TBE running buffer and Agarose SeeGreen

Table 3. Concentration and the purity of the DNA samples on the BlueRay EzDrop Spectrophotometer. The method was dsDNA 50, and the path length was 0.5 mm.

pBAD18-Kan				
Concentration	28.19 ng/µL			
A260	0.56			
A260/A280	2.05			
A260/A320	2.06			
pUS212				
Concentration	12.33 ng/µL			
A260	0.25			
A260/A280	1.57			
A260/A320	1.77			

nucleic acid stain (miniPCR bio kit). Samples were loaded alongside DNA ladders, and

electrophoresis was performed at 60 V for 1 hour. After completion, gels were visualized under blue-light illumination to confirm fragment sizes.

## Results

#### Optical density measurements

After the isolation and purification of the plasmid, the concentration of each plasmid sample was measured with a spectrophotometer. For pBAD18-Kan, a concentration of 28.19 ng/μL was obtained. For pUS212, a concentration of 12.33 ng/μL was obtained.

The purity ratio of pUS212 A260/A280 was lower than that of a DNA that is generally considered pure, with an A260/A280 ratio around or above 1.8. The lower pUS212 A260/A280 ratio indicated that the pUS212 sample was contaminated with other impurities. However, since the number was not excessively off the standard of 1.8, the sample was considered pure enough to continue the lab performance.

#### Verification of the existence of plasmids

The plasmid extractions were subjected to gel electrophoresis to verify the existence of the plasmids, as shown in the figure below. The bands on lane 1 represent a Quick Ladder. On lane 3, the bands represent pUS212. The bands on lane 5 represent a  $\lambda$  ladder, and the bands on lane 7 represent pBAD18-Kan. We confirmed the presence of the purified

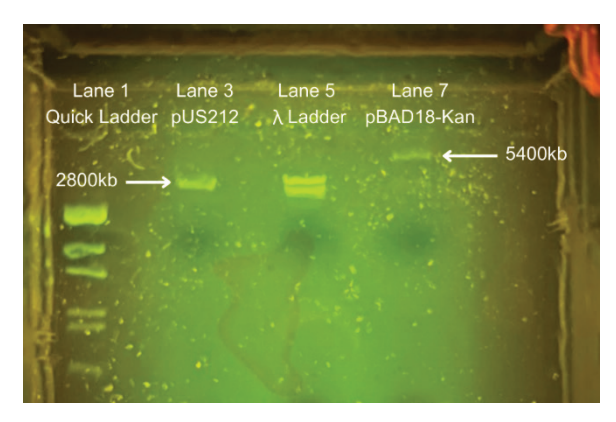


Figure 5. Gel electrophoresis of extracted plasmids.

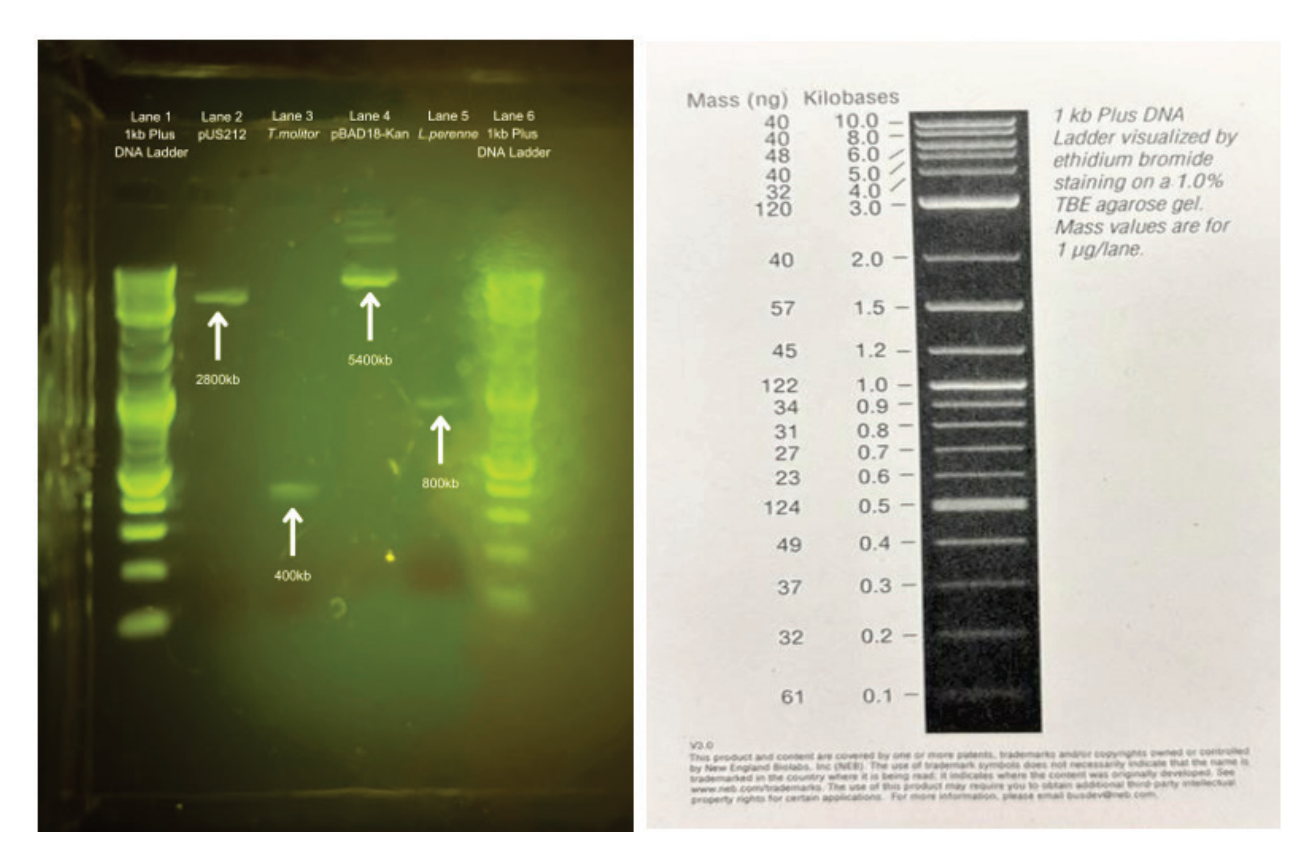


Figure 6. (Left) Gel Electrophoresis of DNA samples of plasmids and inserts, (Right) 1 kb Plus DNA Ladder visualized.

pBAD18-Kan and pUS212 plasmids. The band on lane 3 was observed around 2000 bp, corresponding to the basepair length of pUS212, which is 2808 bp. The band on lane 7 was observed to be around 5000 bp, which corresponds to the basepair length of pBAD18-Kan, which is 5437 bp.

#### Digest analysis

The samples were analyzed by gel electrophoresis after double digestion. Lanes 1 and 6 were run with 1 kb Plus DNA Ladder. On lane 2, the pUS212 sample was run. On lane 3, the *T. molitor* sample was run. On lane 4, the pBAD18-Kan sample was run. On lane 5, the *L. perenne* sample was run. The band on lane 2 was observed around 2 kb, and the band on lane 3 was observed around 0.3 kb. The band on lane 4 was observed around 5 kb, and the band on lane 5 was observed around 0.8 kb. Each lane showed the corresponding result for each sample, matching the DNA length shown on ATCC,

Addgene, and GoldBio. (pUS212–2808 bp, *T. molitor*–378 bp, pBAD18-Kan–5437 bp, *L. perenne*–807 bp).

#### **Transformations**

The transformation of the pUS212 plasmid was successful. Visible colonies were present on all three LA plates, varying in number, size, and volume of the ligations.

For pBAD18-Kan, none of the plates had visible colonies.

#### Results conclusion

Overall, our spectrophotometric measurements and gel analyses confirmed that both pBAD18-Kan and pUS212 plasmids were successfully isolated with adequate purity, and restriction digests produced fragments of the expected sizes for each vector–insert combination. While the TM-AFP construct reliably transformed into DH5-α, there were no LP-AFP colonies.

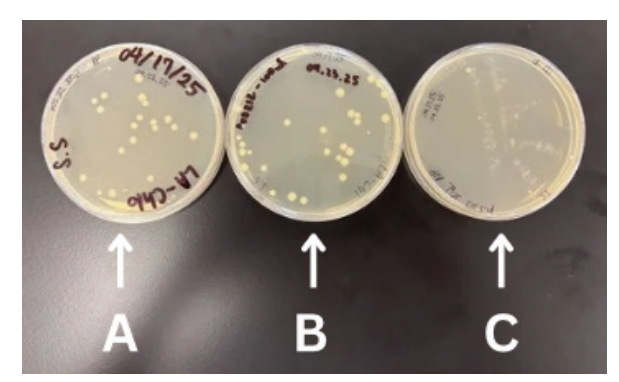


Figure 7. LA plates of DH5- $\alpha$  cells transformed with TM-AFP pUS212. 200  $\mu$ L of transformed cells were plated on plate A, 100 $\mu$ L on plate B, and 20 $\mu$ L on plate C.

# **Discussions**

The goal of this project was to construct two plasmids, one expressing an AFP gene from *L. Perenne* and one from *T. molitor and* then transform them into E. *coli*.

Although protein expression has not yet been achieved at this stage of the project, the progress thus far has been promising. We have successfully designed and synthesized two AFP gene inserts from L. perenne and T. molitor and cloned them into pBAD18-Kan and pUS212 plasmid backbones. The ligation and transformation steps were carried out, and downstream validation was planned through restriction digests to confirm the vector insert combinations. foundational steps provide the potential for moving forward with expression testing in E. coli BL21 (DE3) cells.

In analyzing the results of the current transformation, the LA plates containing DH5-α transformed with TM-AFP pUS212 showed visible colony growth, whereas the LA plates containing DH5-α transformed with LP-AFP pBAD18-Kan exhibited no colony formation. This discrepancy may be attributed to several factors, including issues with plasmid ligation or the concentration of antibiotics used during the selection process. To determine the cause of the transformation failure, we plan to run an agarose gel to verify the DNA content of the ligated vectors and assess the presence of plasmid constructs. If the problem stems from the ligation step, we will review our experimental procedures and



Figure 8. LA plates of DH5- $\alpha$  cells transformed with LP-AFP pBAD18-Kan. 200 μL on two plates on the right, 20 μL on two plates on the left.

choice of restriction enzymes and make any necessary modifications to the experimental design. If ligation appears successful and plasmid DNA is confirmed, we will consult relevant literature to evaluate the performance of the pBAD18-Kan vector under different antibiotic concentrations and adjust our protocol accordingly.

If the BL21 (DE3) expression levels appear suboptimal, which is not uncommon when expressing heterologous proteins in *E. coli* (Rosano & Ceccarelli, 2014), we are prepared to use protein refolding strategies to diminish the impacts of potential inclusion bodies. Specific methods include solubilizing aggregated proteins, gradually renaturing for active protein recovery, and optimizing induction parameters, such as inducer concentration, incubation temperature, and post-induction duration. These conditions will be fine-tuned to minimize stress-induced misfolding.

# **Next steps**

Following overnight incubation, we will select several colonies from the antibiotic-containing plates, which likely harbor successfully ligated plasmids, and culture them in liquid LB media supplemented with the appropriate antibiotics (kanamycin or

chloramphenicol). To verify that the colonies contain plasmids with the correct insert rather than self-ligated vectors, we will isolate plasmid DNA using miniprep and perform analytical restriction digests with the same enzymes used during cloning (NheI/SalI for *L. perenne* AFP and SpeI/PstI for *T. molitor* AFP). Using the original cloning enzymes ensures that only plasmids containing the correctly inserted fragment will be cleaved at the expected sites, producing characteristic band sizes on the gel. The resulting digestion products will be visualized on an agarose gel to confirm the presence and correct orientation of the insert DNA.

Once confirmed, we will scale up the cultures and perform a second round of minipreps to obtain sufficient quantities of recombinant plasmids. These plasmids will be sequenced to verify their structural integrity and then transformed into E. coli BL21 (DE3) cells, a strain optimized for protein expression. To assess the inducibility and optimal expression conditions of the antifreeze proteins, we will test various concentrations of arabinose (for pBAD18-Kan constructs) and tetracycline (for pUS212 constructs). Protein expression levels will be analyzed via SDS-PAGE and Western blotting to determine the efficacy of each build and the conditions that yield the highest expression.

# **Author contributions**

N.P. and L.W. conducted the early research process. A.G., N.P., J.V., and L.W. contributed to the writing and proofreading of the paper. A.G., N.P., J.V., and L.W. created the video. N.P. and L.W. designed the images and graphics for this project.

# **Acknowledgements**

We are grateful to Western Reserve Academy for its generous support and resources. Special thanks to our teacher, Dr. Pethel, for introducing us to the world of synthetic biology and for her guidance and unwavering support throughout the project. We also extend our sincere appreciation to our mentor, Dr. Becky Meyer, whose

thoughtful feedback and continued encouragement helped refine our approach and strengthen our design. Finally, we thank BioBuilder for the invaluable opportunities and support provided throughout this experience.

## References

- American Highway Users Alliance. (2018). Road salt: A primer on the factors affecting supply and demand. https://www.highways.org/wp-content/uploads/2018/12/road-salt-primer-2018.pdf
- American Highway Users Alliance. (n.d.).
  Winter weather highway safety:
  Preventing crashes, injuries and deaths
  [Brochure].
  https://www.highways.org/wpcontent/uploads/2014/02/BrochureFINAL-LoRes.pdf
- Balamurugan, S., Ann, J. S., Varghese, I. P., Murugan, S. B., Harish, M. C., Kumar, S. R., & Sathishkumar, R. (2018). Heterologous expression of lolium perenne antifreeze protein confers chilling tolerance in tomato. *Journal of Integrative Agriculture*, 17(5), 1128-1136. https://doi.org/10.1016/s2095-3119(17)61735-0
- Corsi, S. Ř., De Cicco, L. A., Lutz, M. A., & Hirsch, R. M. (2015). River chloride trends in snow-affected urban watersheds: Increasing concentrations outpace urban growth rate and are common among all seasons. *Science of the Total Environment*, 508, 488-497. https://doi.org/10.1016/j.scitotenv.2014. 12.012
- Eskandari, A., Leow, T. C., Rahman, M. B. A., & Oslan, S. N. (2020). Antifreeze proteins and their practical utilization in industry, medicine, and agriculture. *Biomolecules*, 10(12), 1649. https://doi.org/10.3390/biom10121649
- Gharib, G., Saeidiharzand, S., Sadaghiani, A. K., & Koşar, A. (2022). Antifreeze proteins: A tale of evolution from origin to energy applications. *Front. Bioeng. Biotechnol.* 9:770588. https://doi.org/10.3389/fbioe.2021.770588

- Graham, L. A., Walker, V. K., & Davies, P. L. (2000). Developmental and environmental regulation of antifreeze proteins in the mealworm beetle Tenebrio molitor. *European Journal of Biochemistry*, 267(21), 6452-6458. https://doi.org/10.1046/j.1432-1327.2000.01734.x
- Guidelines for the selection of snow and ice control materials to mitigate environmental impacts. (2007).

  Transportation Research Board. https://doi.org/10.17226/23178
- Hakim, A., Nguyen, J. B., Basu, K., Zhu, D. F., Thakral, D., Davies, P. L., Isaacs, F. J., Modis, Y., & Meng, W. (2013). Crystal structure of an insect antifreeze protein and its implications for ice binding. *Journal of Biological Chemistry*, 288(17), 12295-12304. https://doi.org/10.1074/jbc.m113.450973
- How a Fungi-derived Antifreeze Protein Works: Elucidation of Molecular Structure and Antifreeze Mechanism (Press Release). (2012, May 29). SPring-8. http://www.spring8.or.jp/en/news\_publications/press\_release/2012/120529/
- It makes our roads safer, but is polluting our waterways. (n.d.). Carry Institute of Ecosystem Studies. https://www.caryinstitute.org/our-expertise/freshwater/road-salt
- Kim, H., Lee, J., Hur, Y., Lee, C., Park, S.-H., & Koo, B.-W. (2017). Marine antifreeze proteins: Structure, function, and application to cryopreservation as a potential cryoprotectant. *Marine Drugs*, 15(2), 27.
- https://doi.org/10.3390/md15020027 Kondo, H. (2012, May 29). How an antifreeze protein inhibits ice crystal growth [Illustration]. Spring8. http://www.spring8.or.jp/en/news\_publi cations/press\_release/2012/120529/
- Kuiper, M. J., Davies, P. L., & Walker, V. K. (2001). A theoretical model of a plant antifreeze protein from lolium perenne. *Biophysical Journal*, 81(6), 3560-3565. https://doi.org/10.1016/s0006-3495(01)75986-3
- Kuiper, M. J., Morton, C. J., Abraham, S. E.,

- & Weale, A. G. (2015, May 26). Schematic figure of antifreeze protein (AFP) ice inhibition via the Gibbs—Thomson effect. [Illustration]. *eLife*. https://elifesciences.org/articles/05142
- Lilek, J. (2017, July 13). Roadway deicing in the United States [Fact sheet].

  American Geosciences Institute.

  https://www.americangeosciences.org/geoscience-currents/roadway-deicing-united-states
- Mainroad liquid anti-icing brine program. (n.d.). Mainroad. https://mainroad.ca/mainroad-liquid-anti-icing-brine-program-faq/
- Manual of Practice for an Effective Anti-Icing Program: A Guide for Highway Winter Maintenance Personnel. (1996). U.S. Department of Transportation, Federal Highway Administration. https://www.fhwa.dot.gov/publications/ research/safety/95202/002.cfm
- Middleton, A. J., Brown, A. M., Davies, P. L., & Walker, V. K. (2009). Identification of the ice-binding face of a plant antifreeze protein. *FEBS Letters*, 583(4), 815-819. https://doi.org/10.1016/j.febslet.2009.01.035
- Pieper, K. J., Tang, M., Jones, C. N., Weiss, S., Greene, A., Mohsin, H., Parks, J., & Edwards, M. A. (2018). Impact of road salt on drinking water quality and infrastructure corrosion in private wells. *Environmental Science & Technology*, 52(24), 14078-14087.
- https://doi.org/10.1021/acs.est.8b04709
  Pudney, P., Buckley, S., Sidebottom, C.,
  Twigg, S., Sevilla, M.-P., Holt, C.,
  Roper, D., Telford, J., McArthur, A., &
  Lillford, P. (2003). The physicochemical characterization of a boiling
  stable antifreeze protein from a
  perennial grass (Lolium perenne).

  Archives of Biochemistry and
  Biophysics, 410(2), 238-245.
  https://doi.org/10.1016/s00039861(02)00697-5
- Puetz, J., & Wurm, F. M. (2019).
  Recombinant proteins for industrial versus pharmaceutical purposes: A review of process and pricing.
  Processes, 7(8), 476.
  https://doi.org/10.3390/pr7080476

#### BioTreks

Rosano, G. L., & Ceccarelli, E. A. (2014). Recombinant protein expression in escherichia coli: Advances and challenges. *Frontiers in Microbiology*, 5:172. https://doi.org/10.3389/fmicb.2014.00172

Walters, K. R., Serianni, A. S., Sformo, T.,

Barnes, B. M., & Duman, J. G. (2009). A nonprotein thermal hysteresis-producing xylomannan antifreeze in the freeze-tolerant Alaskan beetle Upis ceramboides. *Proceedings of the National Academy of Sciences*, 106(48), 20210-20215. https://doi.org/10.1073/pnas.090987216